

# Supplementary information for Trithiocarbonate-functionalized PNiPAAm-based nanocomposites for antimicrobial properties

Milène Tan<sup>a</sup>, Lenke Horvath<sup>a</sup>, Priscilla S. Brunetto<sup>a</sup>, Katharina M. Fromm<sup>a\*</sup>

<sup>a</sup>University of Fribourg, Department of Chemistry, Chemin du Musée, 9. 1700 Fribourg, Switzerland.

E-mail: Katharina.fromm@unifr.ch

## Table of contents

### 1\ Structural characterization of the polymers and the nanocomposites

1.1 <sup>1</sup> H-NMR-spectra of the poly(N-isopropylacrylamide)'s.....	S1-4
1.2 FT-IR spectra of the nanocomposites B, C and D.....	S5-7
1.3 UV-Vis spectra of the nanocomposites with the ratio (3).....	S8
1.4 Thermoreversible behavior studied by UV-vis upon heating-cooling cycles.....	S9-11
1.4 X-ray diffractogram of the polymer B and the nanocomposites.....	S12
1.5 TEM micrographs of the polymer B, C, D and the nanocomposites.....	S13-15

### 2\ Thermal properties

2.1 TGA curves of the polymers B, C and D and the nanocomposites.....	S16-18
2.2 DSC traces of the polymers B, C and D and the nanocomposites.....	S19-21
2.3 LCST behaviors of the polymers B and C and the nanocomposites.....	S22

### 3\ Stability studies

3.1 For all the nanocomposites the ratio (3) and (4) in H <sub>2</sub> O.....	S23-24
3.2 For the polymers B and C with the ratio (3) in PBS.....	S25

### 4\ Release kinetics

4.1. Silver release profile of nanocomposite B and C.....	S26-27
4.2. Silver release profile of nanocomposite A, B, C and D.....	S28-31

### 5\ Antimicrobial properties for the polymers

5.1. Killing curves of the nanocomposite B and C with <i>E. coli</i> .....	S32-33
5.2. Killing curves of the nanocomposite B and C with <i>S. aureus</i> .....	S34-35

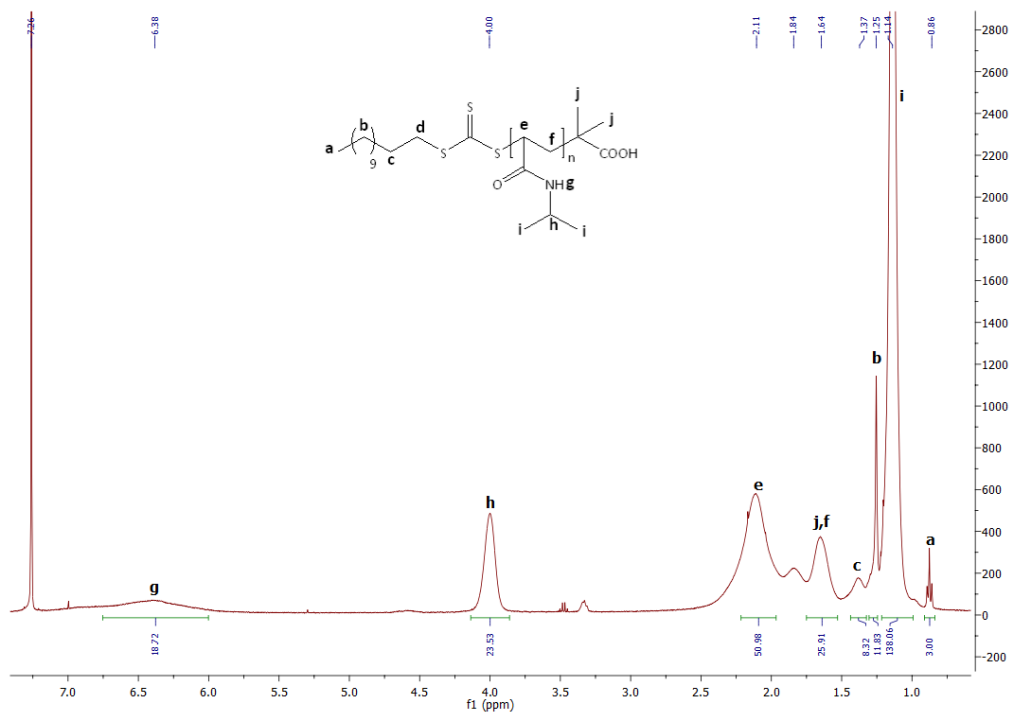


Fig. S1 <sup>1</sup>H-NMR (400 MHz) spectrum of the polymer A

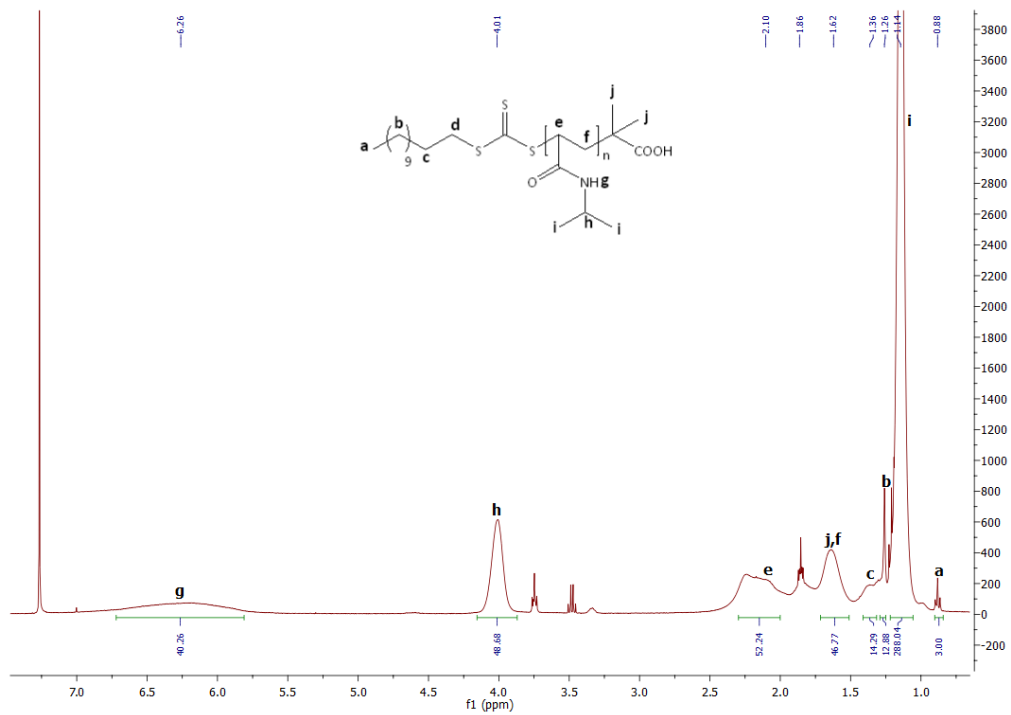


Fig. S2 <sup>1</sup>H-NMR (400 MHz) spectrum of the polymer B

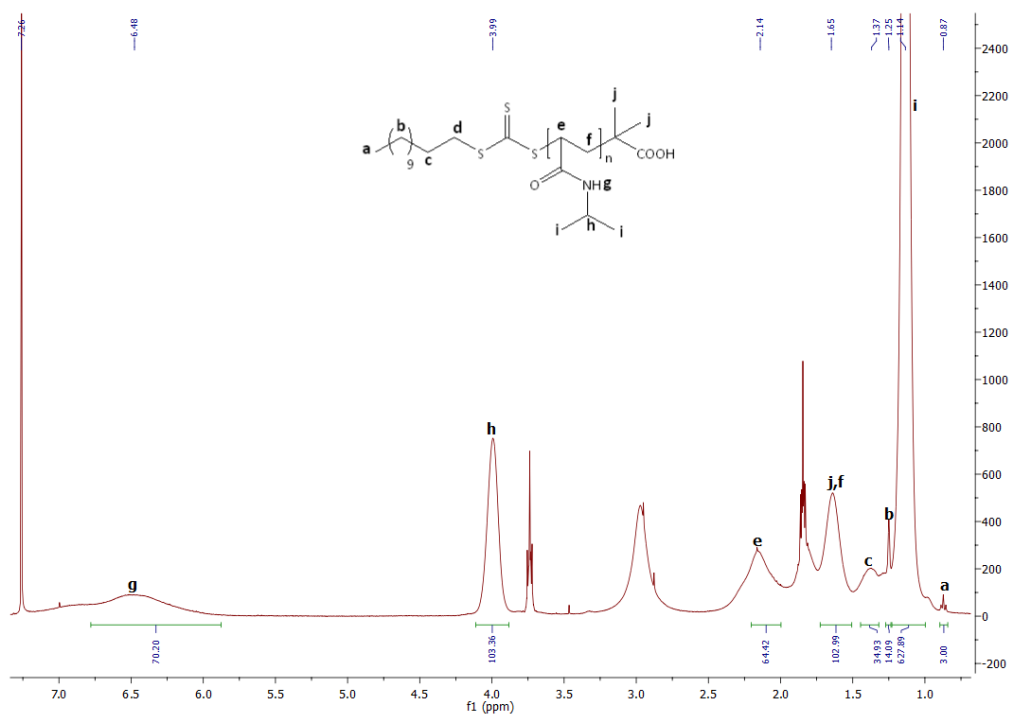


Fig. S3 <sup>1</sup>H-NMR (400 MHz) spectrum of the polymer C

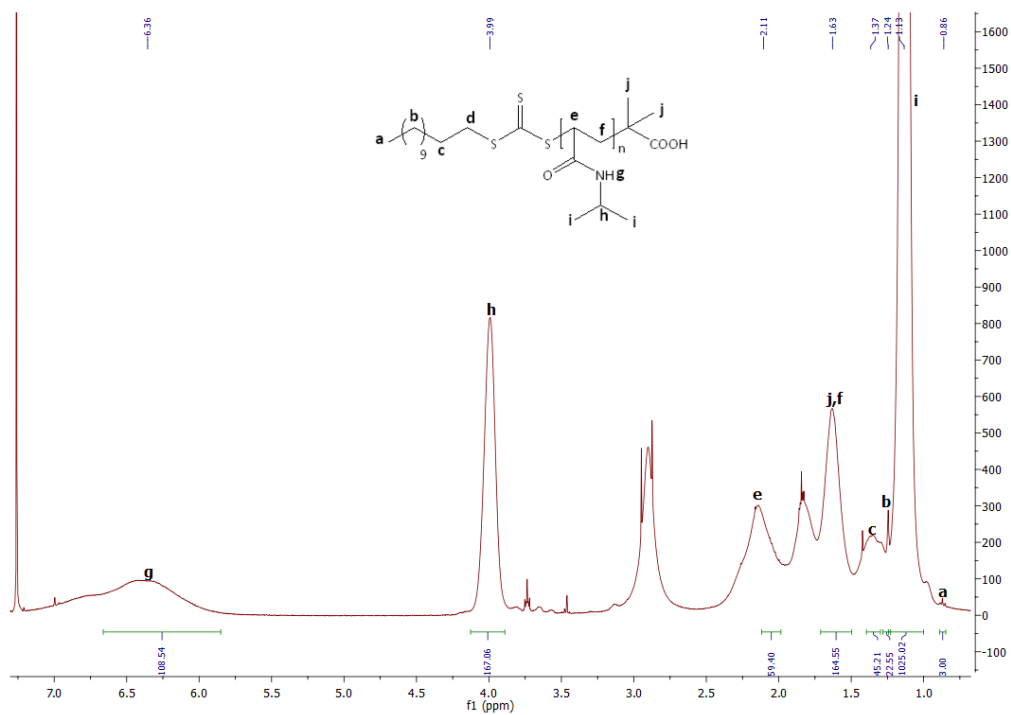


Fig. S4 <sup>1</sup>H-NMR (400 MHz) spectrum of the polymer D

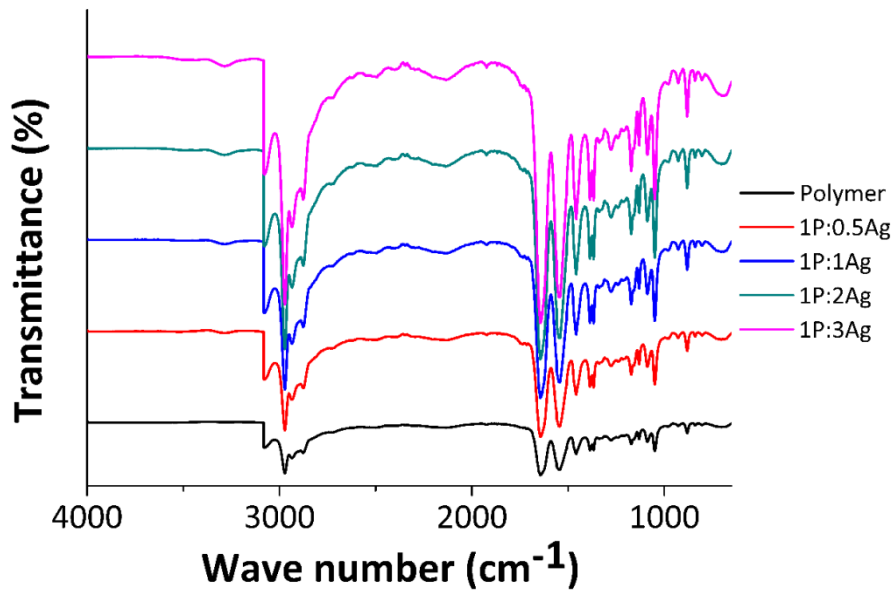


Fig. S5: FT-IR spectra of the polymer **B** and the nanocomposites

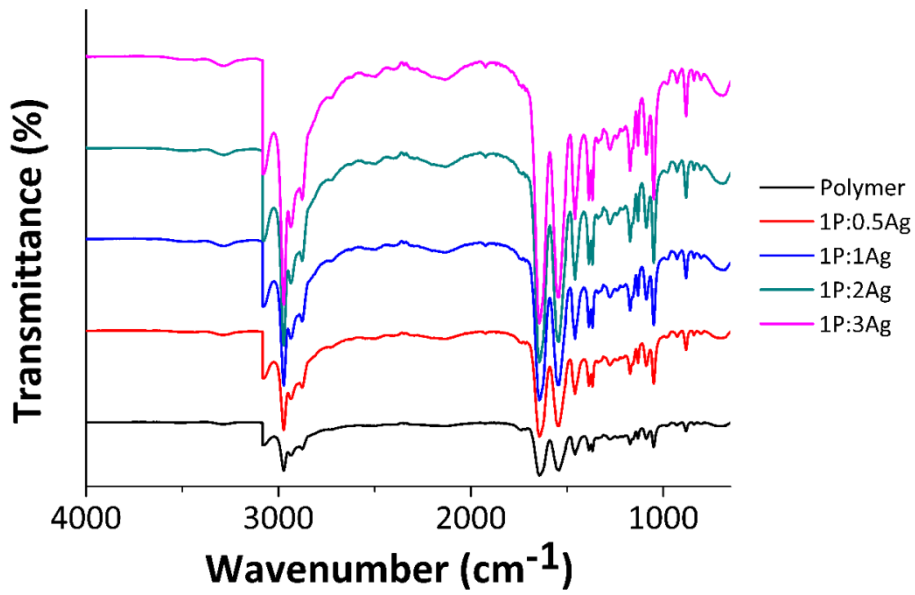


Fig. S6 : FT-IR spectra of the polymer **C** and the nanocomposites

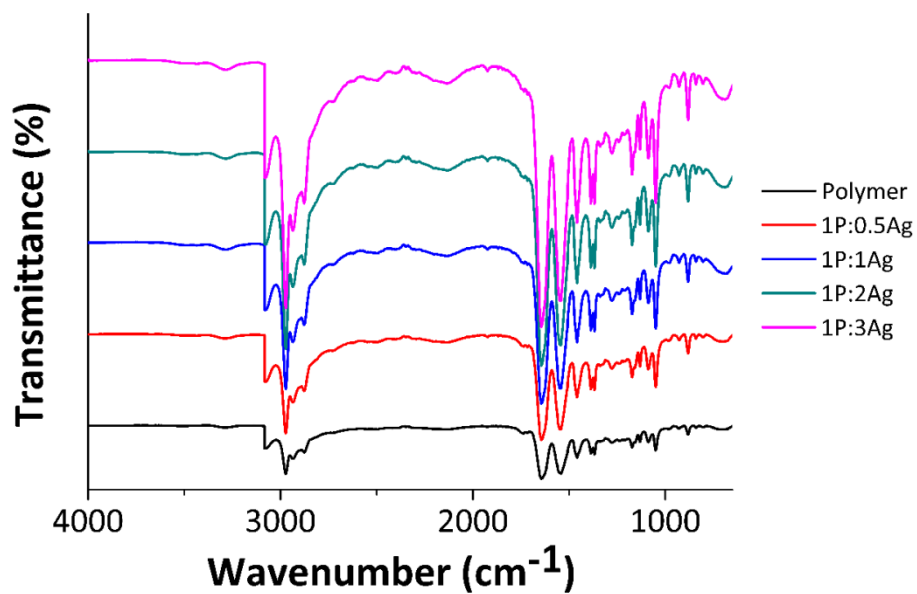


Fig. S7 : FT-IR spectra of the polymer D and the nanocomposites

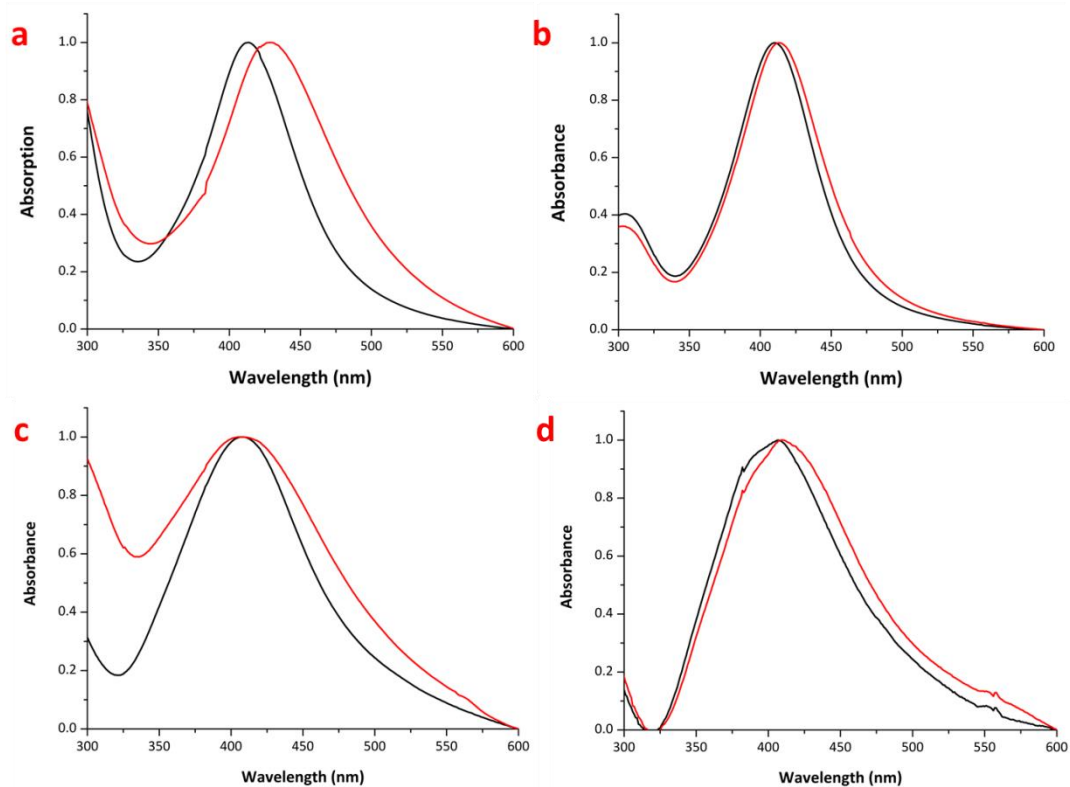


Fig. S8: UV-vis spectra of the nanocomposites a) polymer A, b) polymer B, c) polymer C, d) polymer D with the ratio (3) at RT (black) and 37 °C (red)

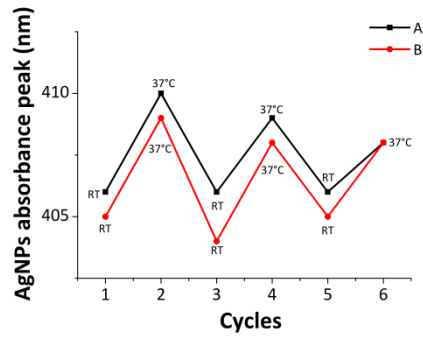


Fig. S9 Thermoreversible behavior studied by UV-vis for the polymer **B** with the ratios **(3)** (A) and **(4)** (B)

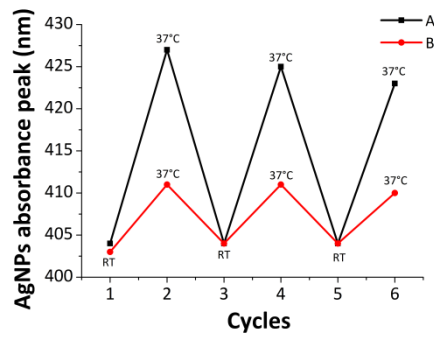


Fig. S10 Thermoreversible behavior studied by UV-vis for the polymer **C** with the ratios **(3)** (A) and **(4)** (B)

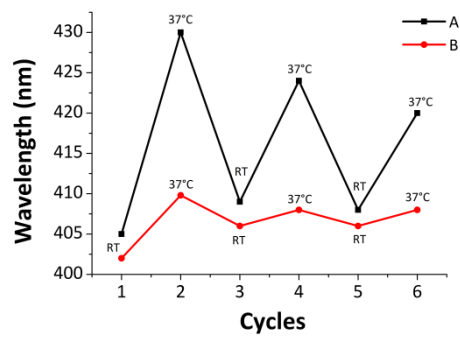


Fig. S11 Thermoreversible behavior studied by UV-vis for the polymer **C** with the ratios **(3)** (A) and **(4)** (B)

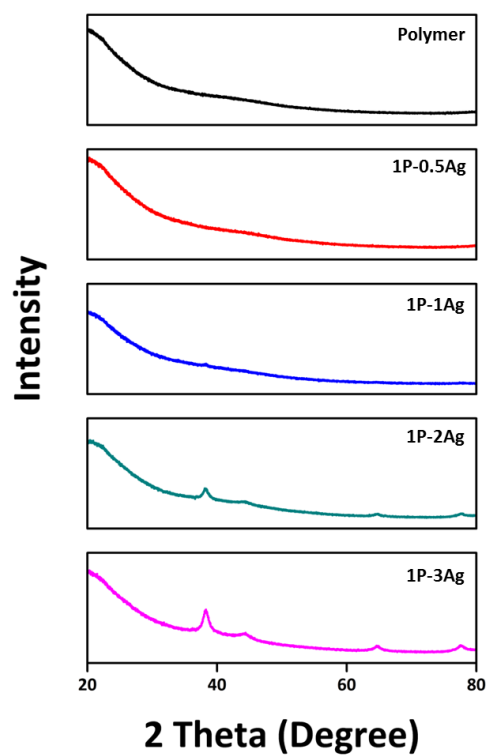


Fig. S12 X-ray diffractogram of the polymer **B** and the nanocomposites

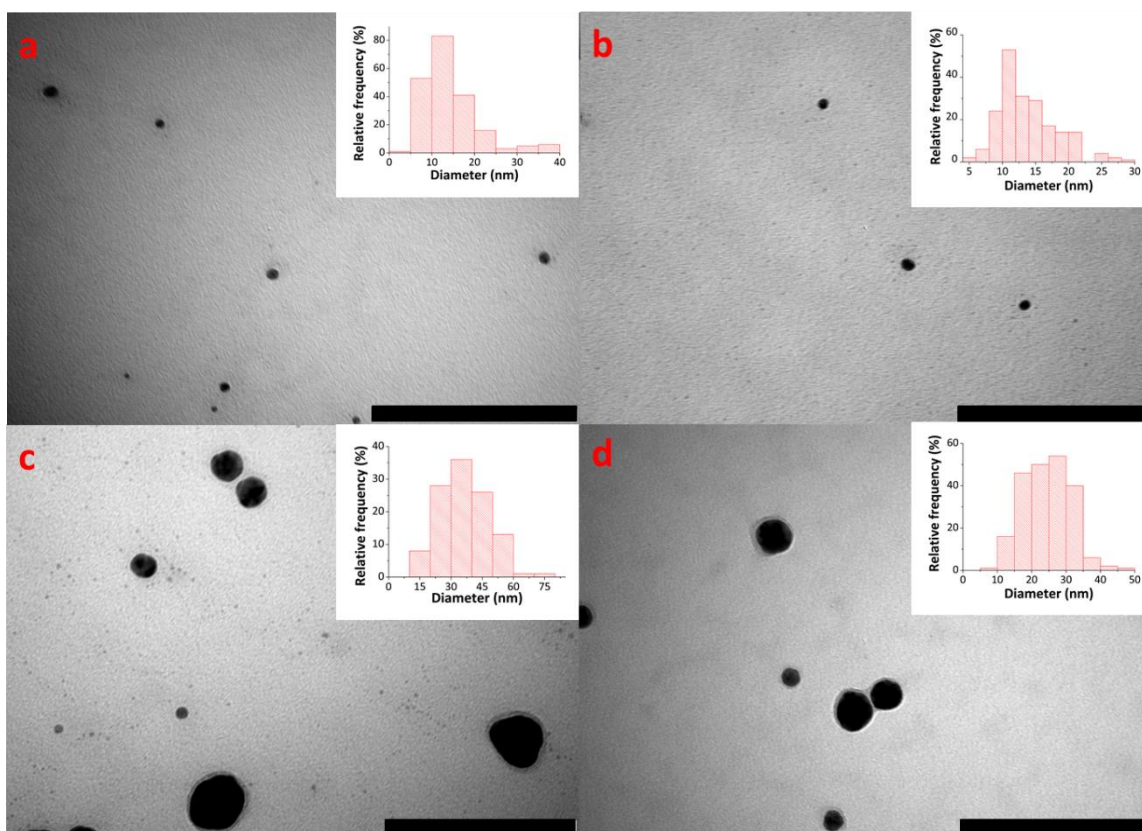


Fig. S13 TEM micrographs and distribution of the nanoparticles for the nanocomposites **B** with the different ratios (1) (a) (203 NPs), (2) (b) (208 NPs), (3) (c) (113 NPs), (4) (d) (216 NPs).

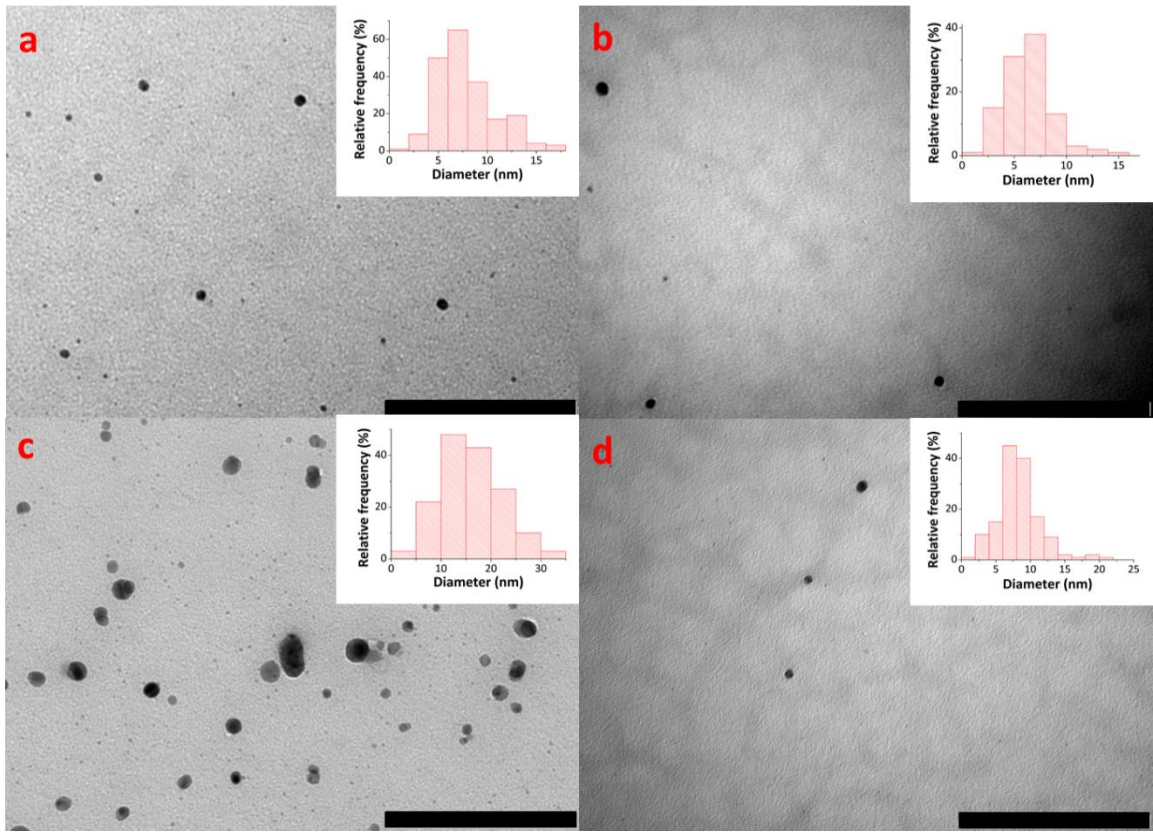


Fig. S14 TEM micrographs and distribution of the nanoparticles for the nanocomposites **C** with the different ratios (1) (a) (205 NPs), (2) (b) (105 NPs), (3)(c) (156 NPs), (4) (d) (143 NPs)

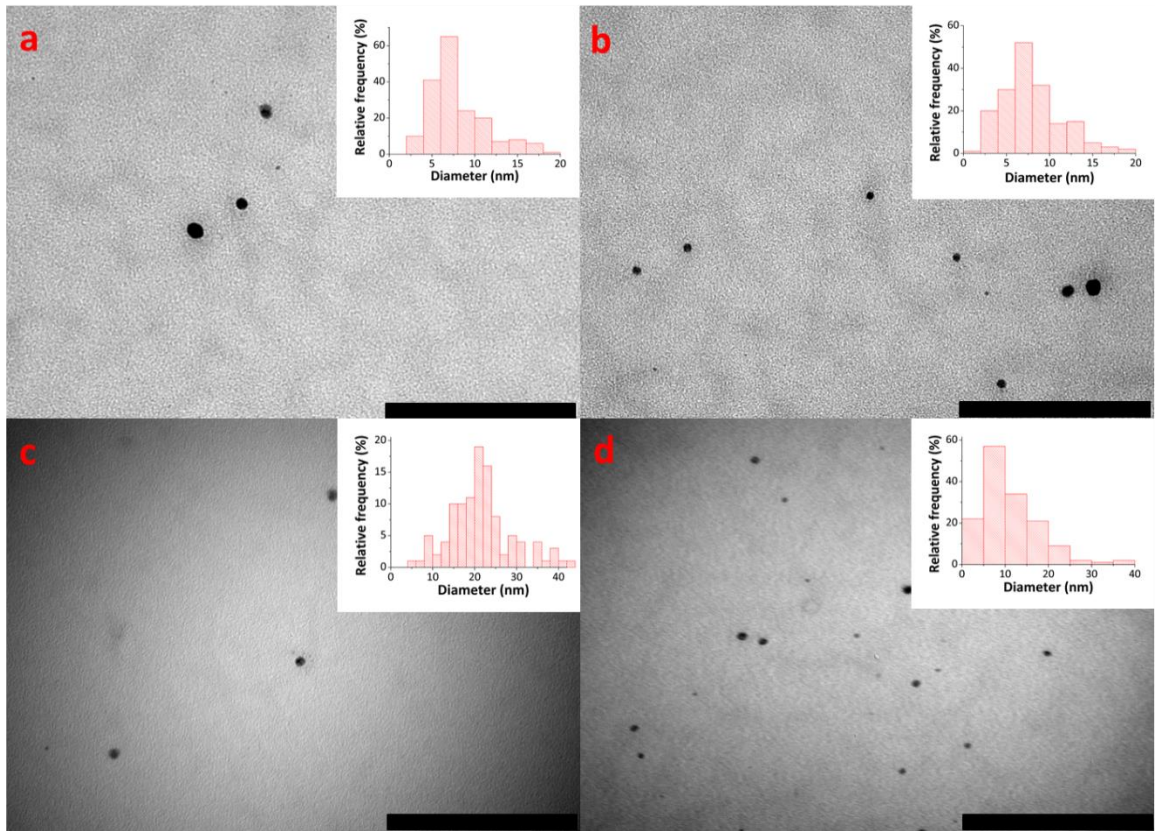


Fig. S15 TEM micrographs and distribution of the nanoparticles for the nanocomposites **D** with the different ratios (1) (a) (182 NPs), (2) (b) (174 NPs), (3)(c) (108 NPs), (4) (d) (148 NPs).



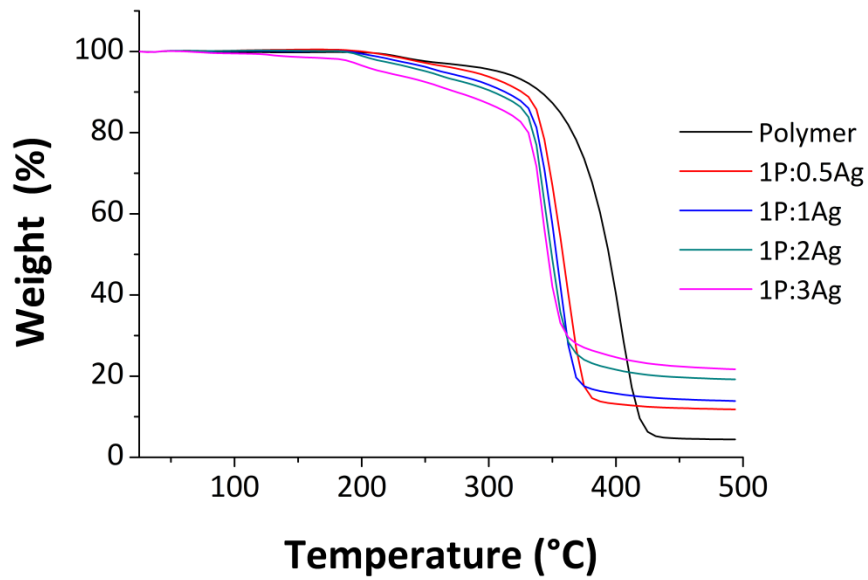


Fig. S16 TGA traces of the polymer **B** and the nanocomposites

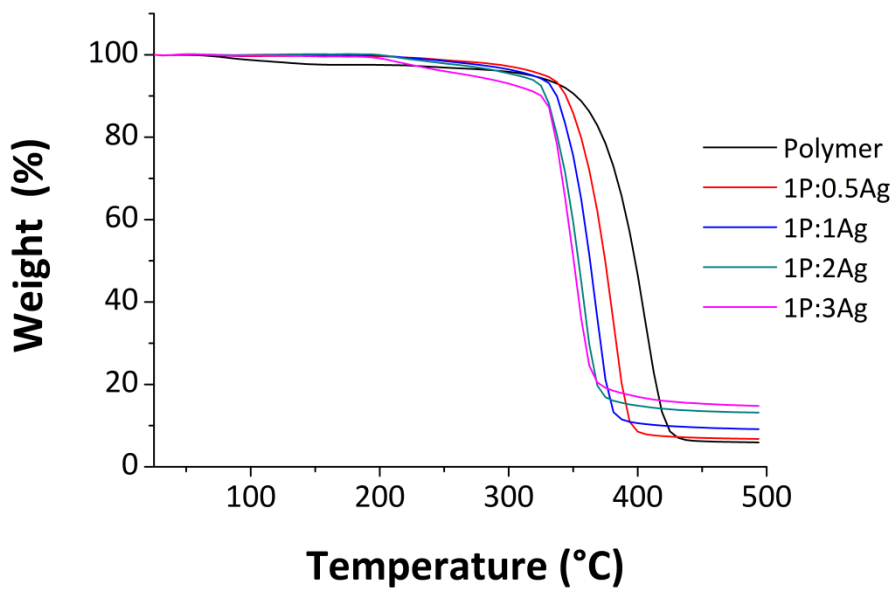


Fig. S17 TGA traces of the polymer **C** and the nanocomposites

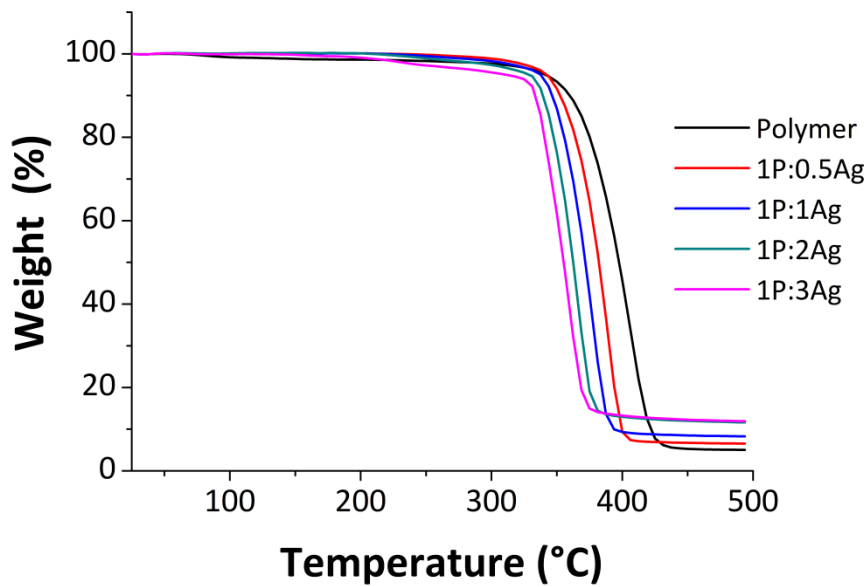


Fig. S18 TGA traces of the polymer D and the nanocomposites

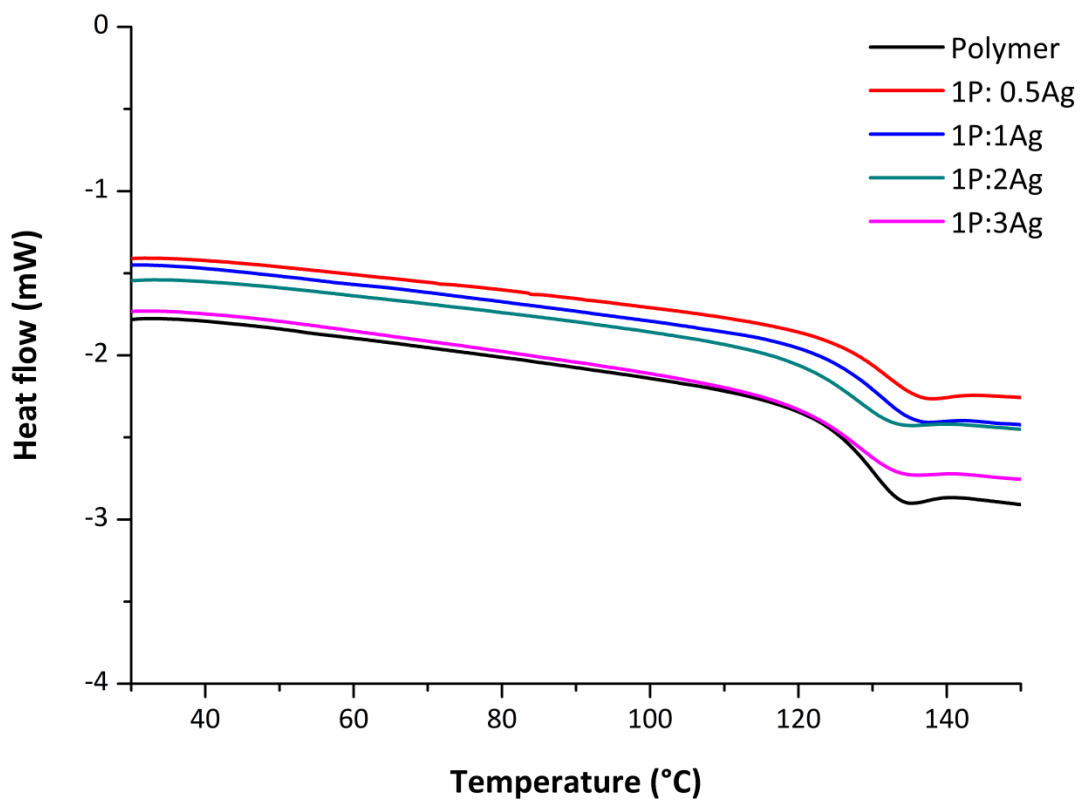


Fig. S19 DSC curves of the polymer B and the nanocomposites

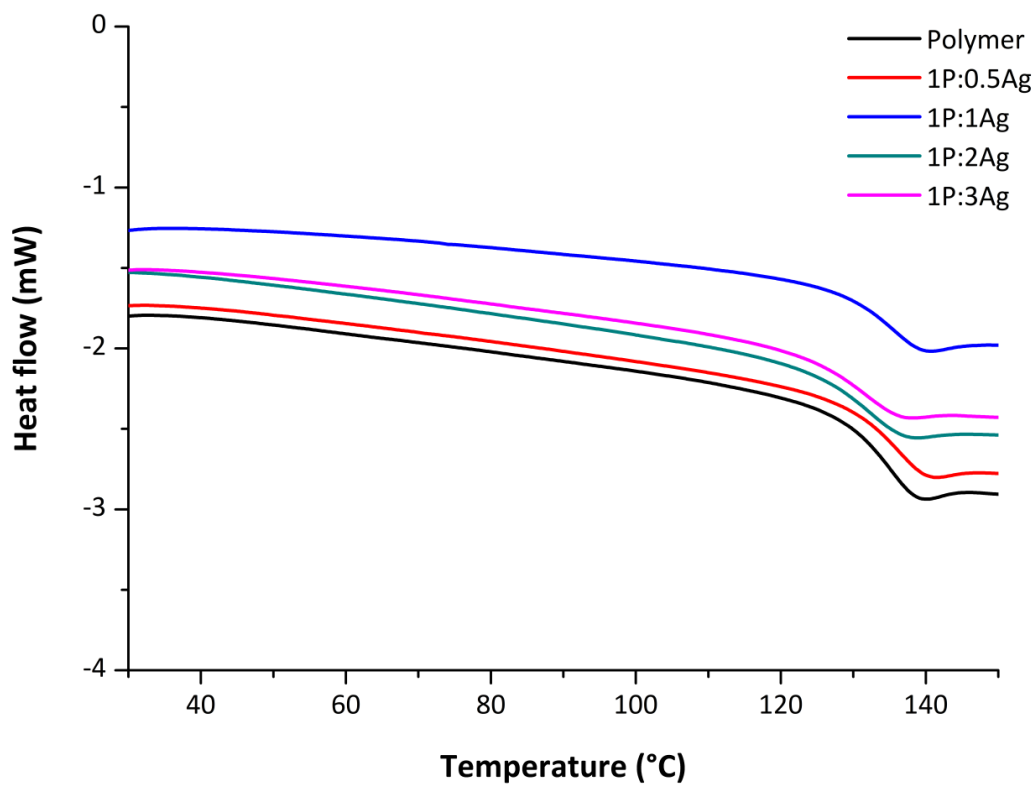


Fig. S20 DSC curves of the polymer C and the nanocomposites

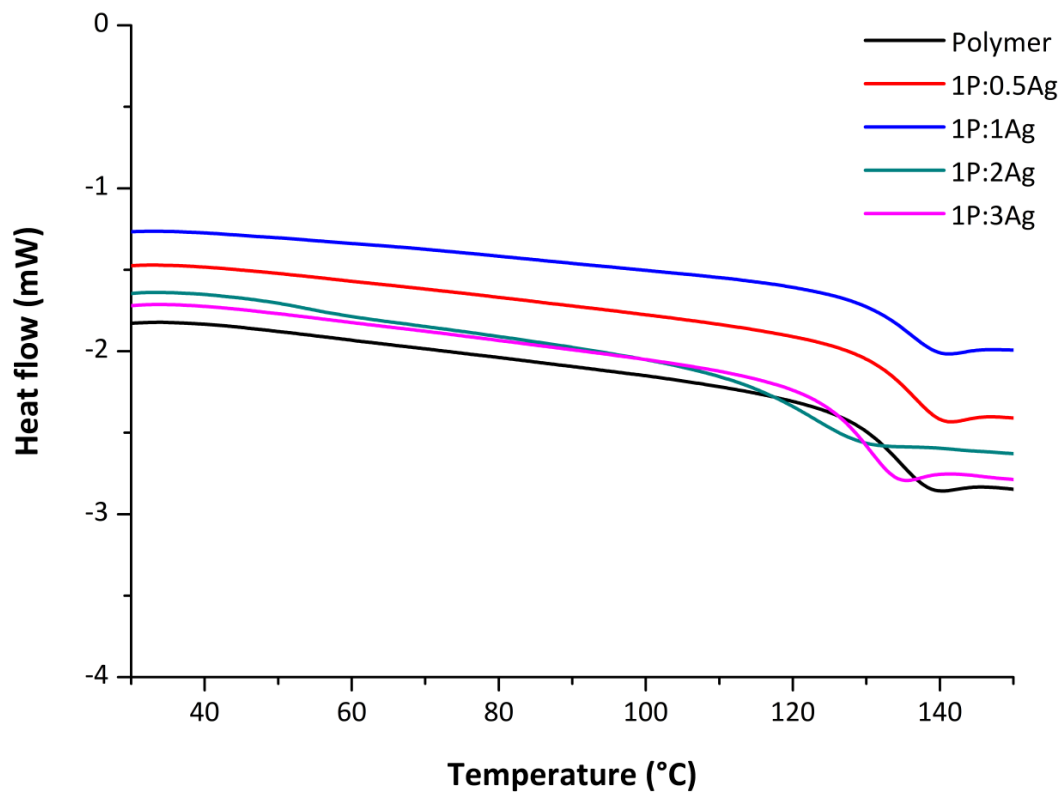


Fig. S21 DSC curves of the polymer D and the nanocomposites

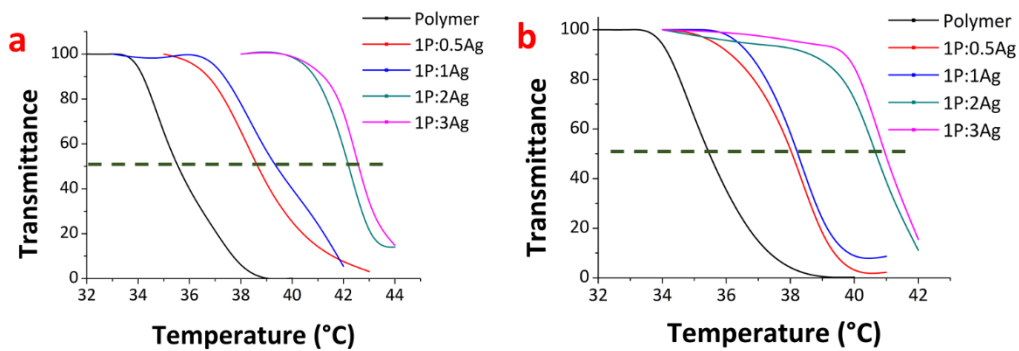


Fig. S22 LCST behaviors of the polymer and the nanocomposites B (left) and C (right)

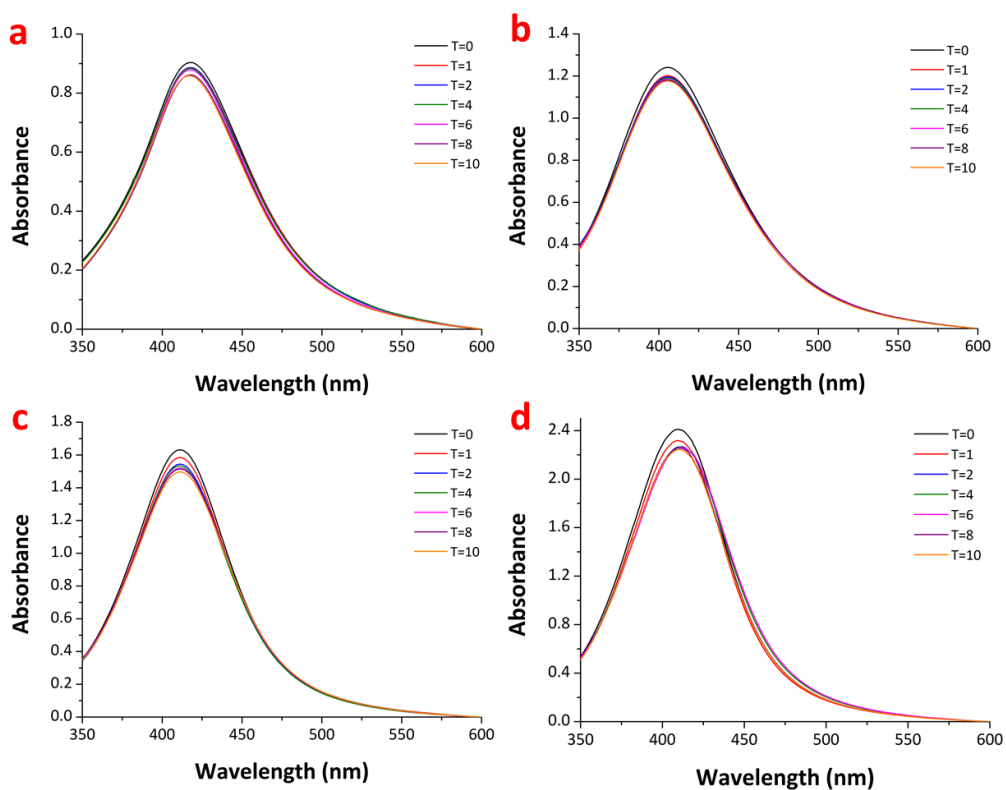


Fig. S23 Stability studies for polymer A (up) and B (down) with the ratio (2) (a, c) and (3) (b, d) in H<sub>2</sub>O

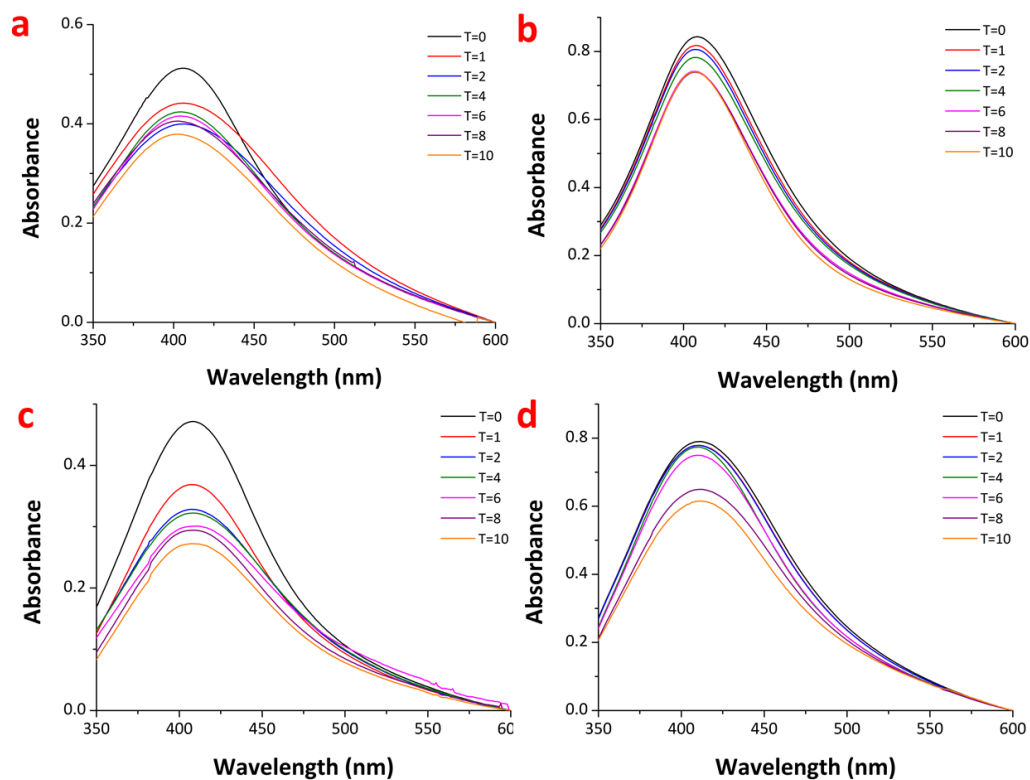


Fig. S24 Stability studies for polymer C (up) and D (down) with the ratio (2) (a, c) and (3) (b, d) in H<sub>2</sub>O

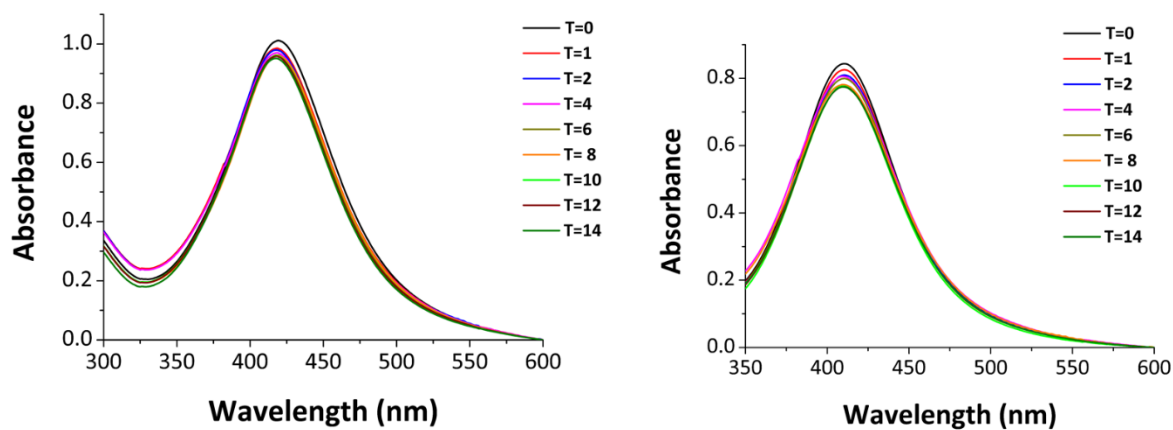


Fig. S25 Stability studies for the ratio (3) with polymer A (left) and B (right) in PBS

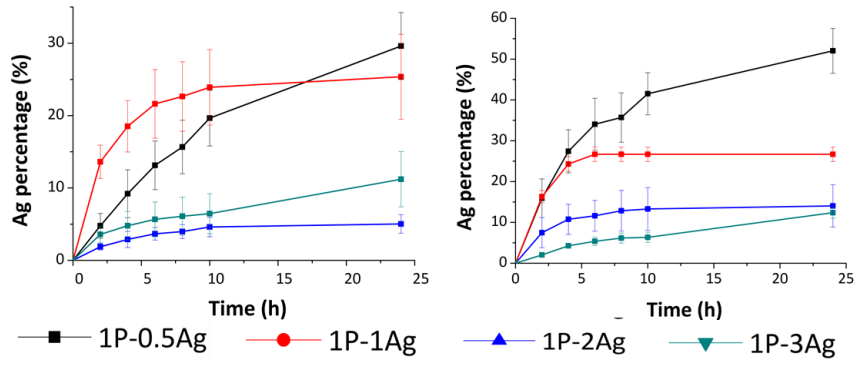


Fig. S26  $\text{Ag}^+$  release kinetics of the nanocomposites **B** at RT (left) and at 37 °C (right)

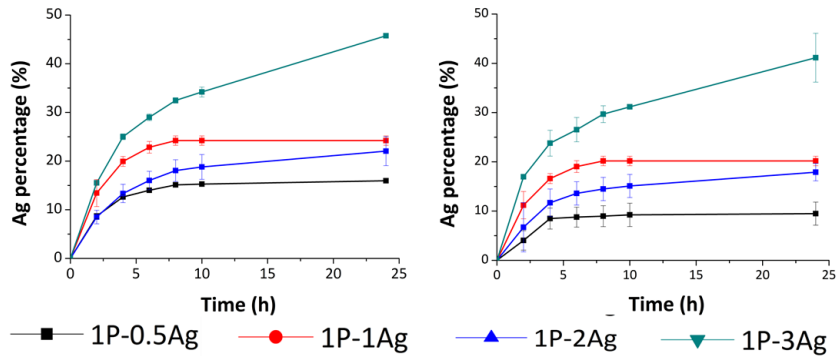


Fig. S27  $\text{Ag}^+$  release kinetics of the nanocomposites **C** at RT (left) and at 37 °C (right)

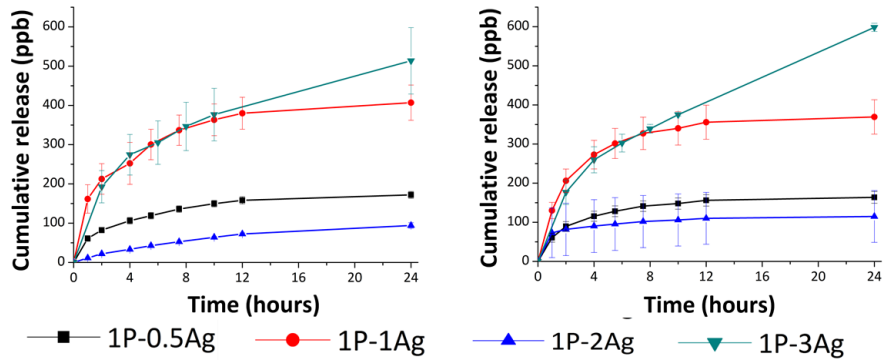


Fig. S28  $\text{Ag}^+$  release kinetics of the nanocomposites **A** at RT (left) and at 37 °C (right)

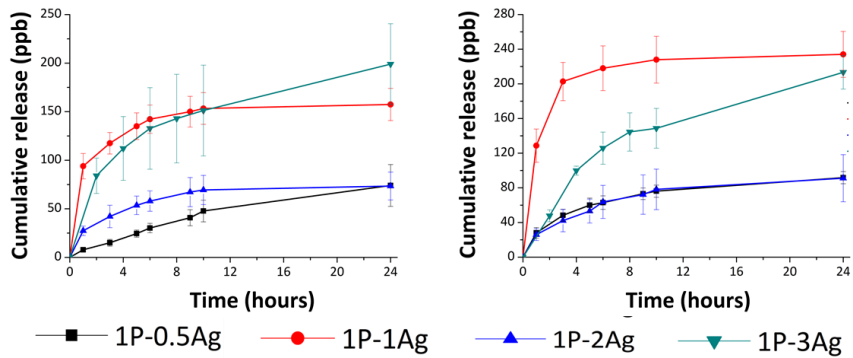


Fig. S29 Release kinetics of the nanocomposites **B** at RT (left) and at 37 °C (right)

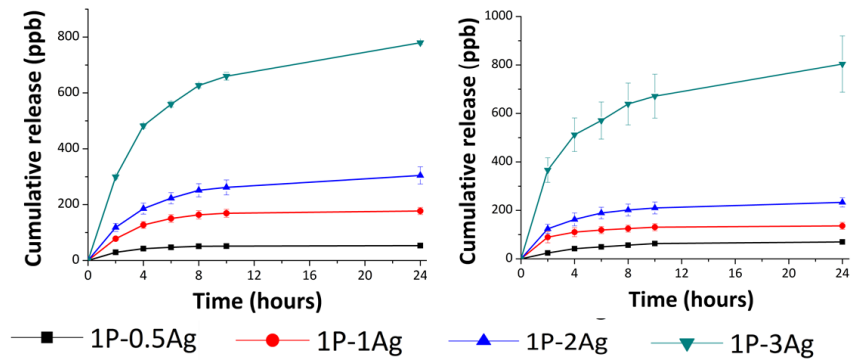


Fig. S30  $\text{Ag}^+$  release kinetics of the nanocomposites **C** at RT (left) and at  $37^\circ\text{C}$  (right)

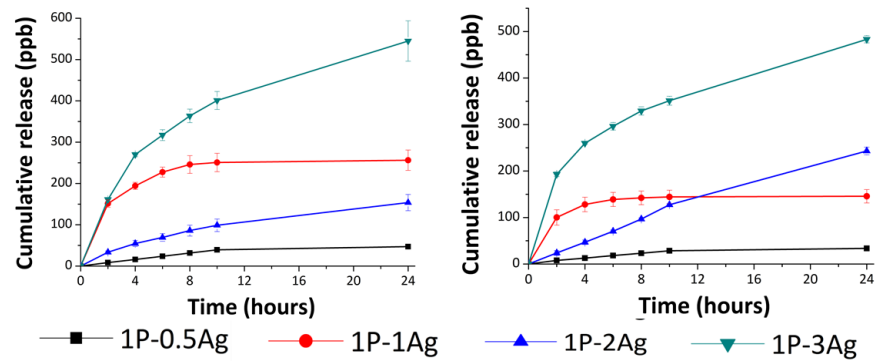


Fig. S31  $\text{Ag}^+$  release kinetics of the nanocomposites **D** at RT (left) and at  $37^\circ\text{C}$  (right)

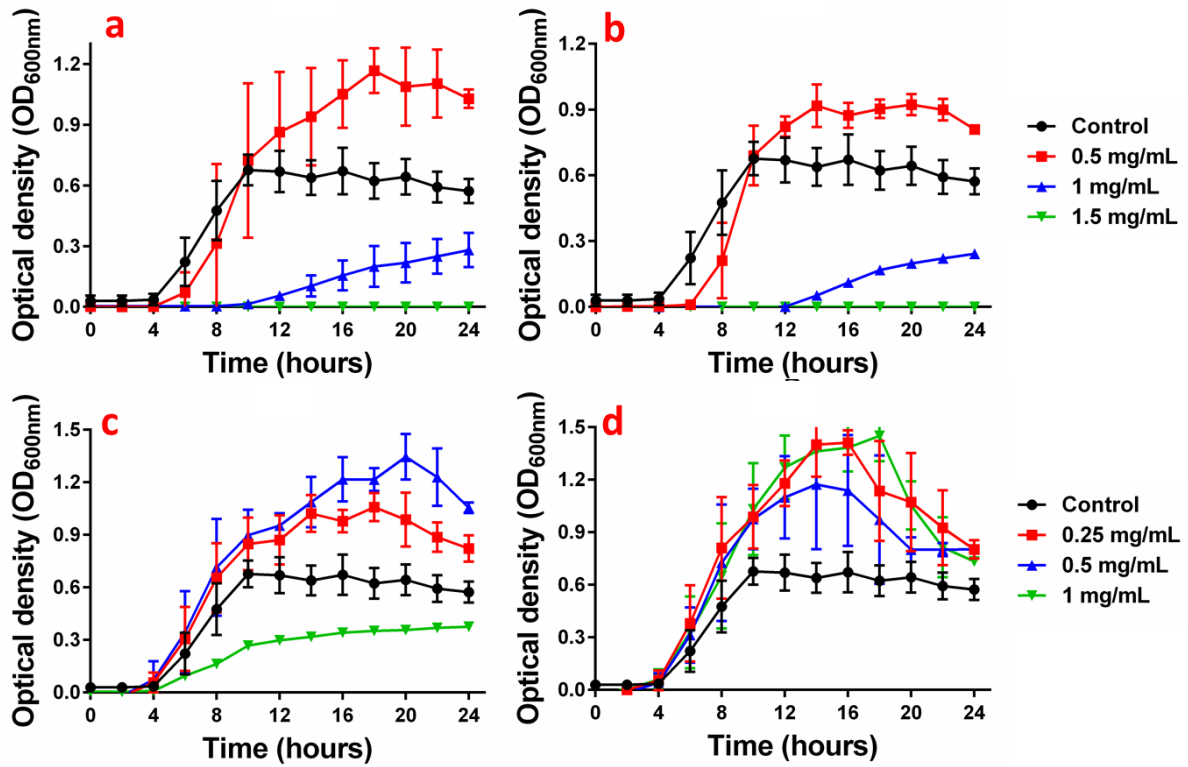


Fig. S32 Growth curves of the nanocomposites B with the different ratios (1) (a), (2) (b), (3) (c), (4) (d) at various concentrations against *E. Coli*

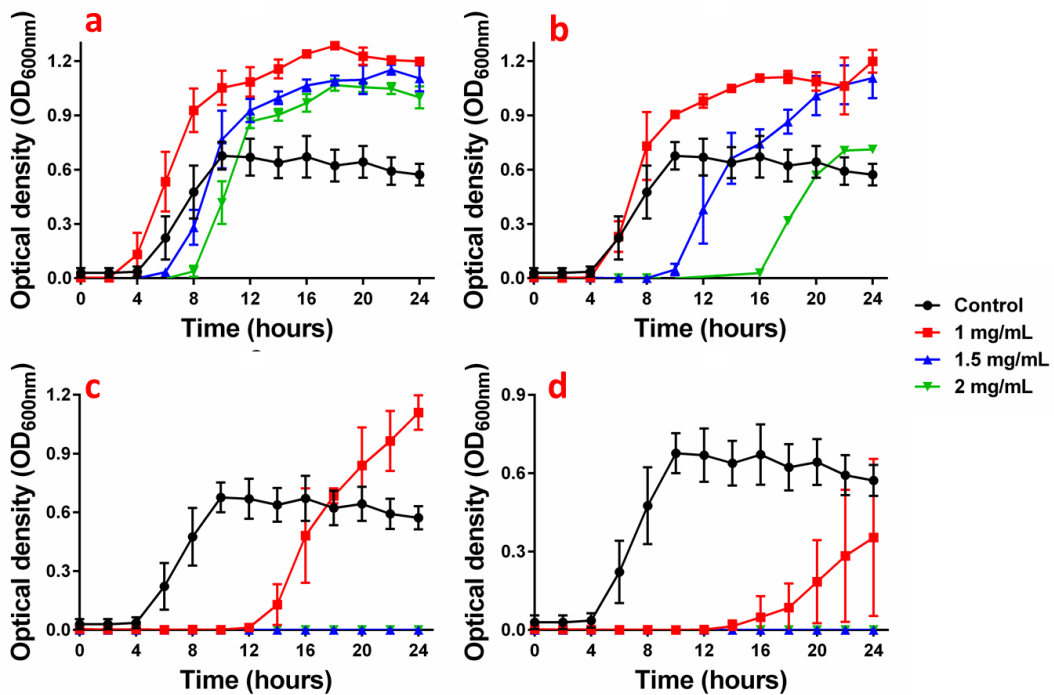


Fig. S33 Growth curves of the nanocomposites C with the different ratios (1) (a) (2) (b), (3) (c), (4) (d) at various concentrations against *E. Coli*



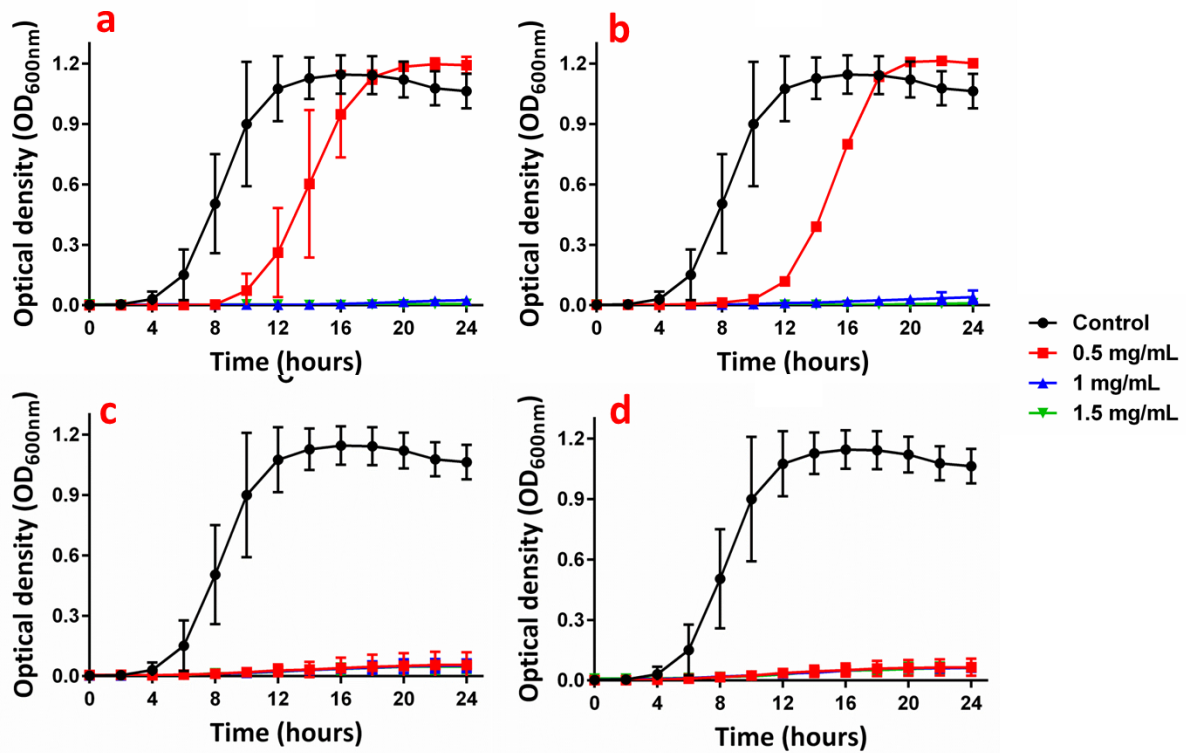


Fig. S34 Growth curves of the nanocomposites **B** with the different ratios (1) (a) (2) (b), (3) (c), (4) (d) at various concentrations against *S. aureus*

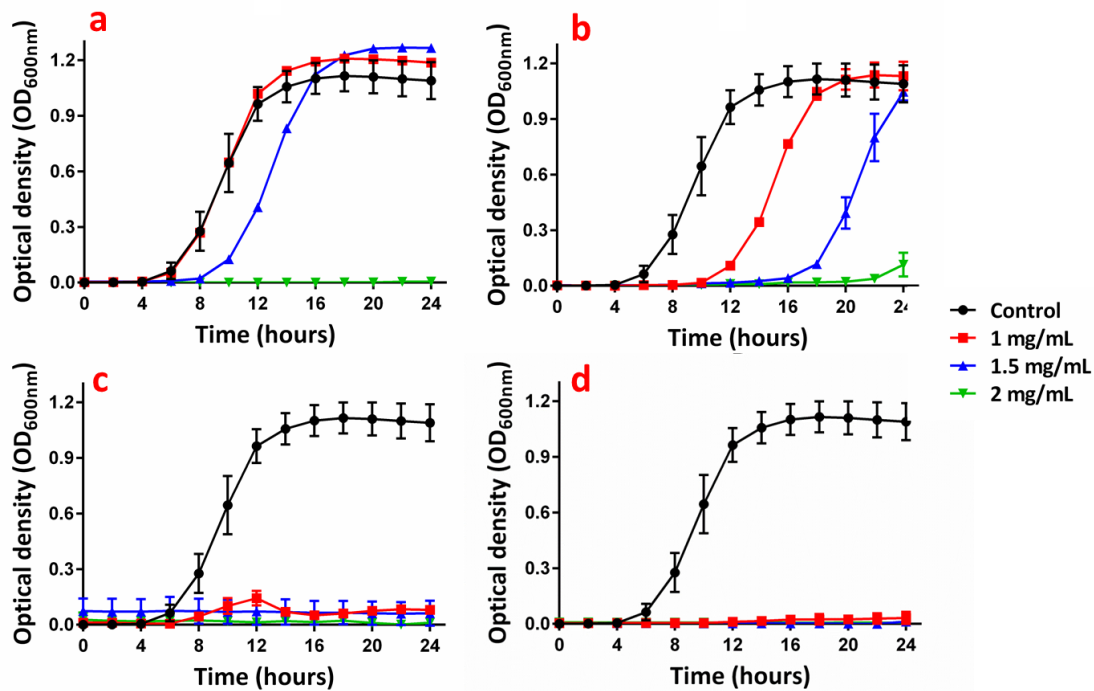


Fig. S35 Growth curves of the nanocomposites **C** with the different ratios (1) (a) (2) (b), (3) (c), (4) (d) at various concentrations against *S. aureus*